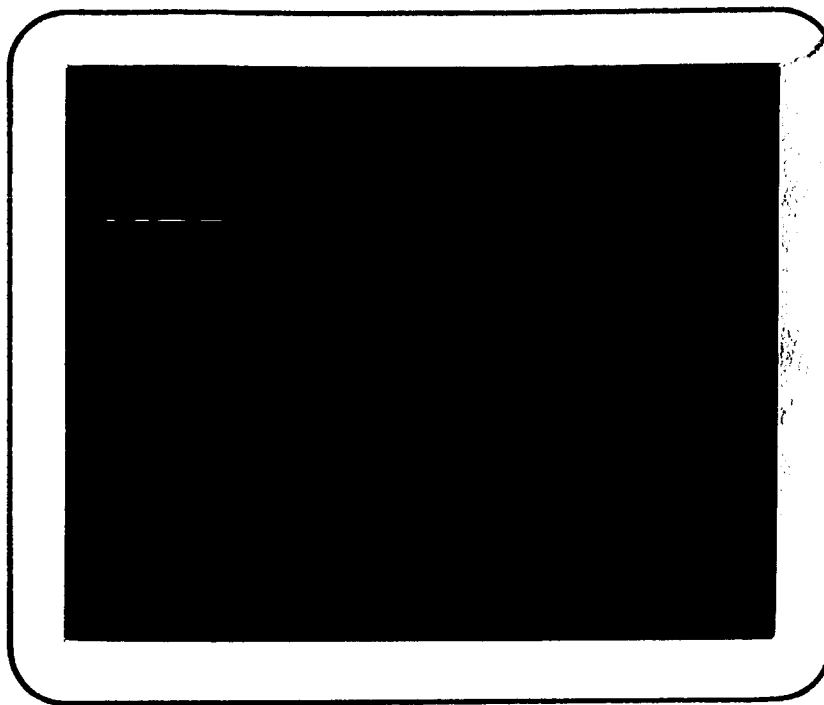


2  
(NASA-CR-123817) OPTIMAL BRAKING STUDIES  
Final Summary Report, 1 Feb. - 15 Aug. 1972  
J.S. Pazdera (Missouri Univ.) 15 Aug. 1972  
50 p  
CSCL 13I

N72-31279

G3/10 Unclas  
41566



 *Department of*

# ELECTRICAL ENGINEERING

CONTROL AND SYSTEMS STUDIES



## University of Missouri - Rolla

Reproduced by  
NATIONAL TECHNICAL  
INFORMATION SERVICE  
U S Department of Commerce  
Springfield VA 22151

5078

OPTIMAL BRAKING STUDIES

prepared by:  
John S. Pazdera

CR-123817  
Final Summary Report

NAS8-28230

1 FEB 72 thru 15 AUG 72

University of Missouri - Rolla  
Department of Electrical Engineering  
Rolla, Missouri 65401

Prepared for the George C. Marshall  
Space Flight Center, NASA, Marshall Space  
Flight Center, Alabama 35812

TABLE OF CONTENTS

SUMMARY OF CONTRACT WORK . . . . .	ii
RECOMMENDATIONS . . . . .	iv
ACKNOWLEDGEMENTS . . . . .	v
ADAPTIVE BRAKING SYSTEM . . . . .	1
Introduction . . . . .	1
I. Development of a peak-riding adaptive controller . . . . .	2
II. Application with simulation results .	6
III. Practical considerations . . . . .	10
Conclusions . . . . .	14
References . . . . .	15
Figures 1 through 14 . . . . .	16
APPENDIX A. Details of analog simulation . . .	31
APPENDIX B. Additional simulation data . . . .	37
APPENDIX C. Mu - slip anomaly . . . . .	40
final page . . . . .	44

### SUMMARY OF CONTRACT WORK

Early in the contract period much effort was spent trying to approach the minimum distance braking without excessive tire wear problem as an optimal regulator problem with unknown disturbance. No significant results were obtained even when the disturbance was assumed known. Effort was then diverted to development of an adaptive, peak-riding controller in order to produce some practical, near-optimal results which was the primary charge of the contract.

The main body of this report describes the peak-riding, adaptive controller designed to provide minimum distance braking of vehicles which obtain their deceleration from frictional forces between the tire and pavement. Organization of this part of the final report is discussed in the Introduction.

Simulation studies were made on the IBM 360/50 with CSMP and on the UMR TR-48/SCC-650 hybrid computer. CSMP was used to study not only the rigid body and strut bending dynamics of a braking airplane, but also the tire to wheel rotational dynamics which forced the time steps to be in the order of milli-seconds. Hence, the

average landing cost about \$25 in cpu time, not including the cost of data plotting.

As the computer funds rapidly disappeared, the analog computer program was developed. All simulation results in the final report were obtained from the TR-48/SCC-650 hybrid computer. Complete details of the analog simulation are reported in Appendix A. Real-time results were displayed on an oscilloscope. To produce X-Y plots for the report, a time scale factor of 50 was used. Landing time was then about 3 minutes, still faster than CSMP compute time.

Numerous simulation runs were made, each providing additional information about the performance of the system. Significant results not covered in the main body of the report are discussed in Appendix B.

Early in the contract, an apparent anomaly was discovered in mu-slip data normally assumed by investigators of braking systems. Appendix C presents a possible explanation of the anomaly, although experimentation is necessary prior to drawing any conclusions about the hypothesis in Appendix C.

## RECOMMENDATIONS

Since the controller developed during this study is applicable to most of the significant modes of transportation in the United States (e.g. airplane, auto, truck, train, and motorcycle), an experimental braking system should be developed and tested for at least one of the above vehicles. Safety of passengers, crew, and innocent victims of accidents resulting from loss of vehicle control during braking is the primary justification for continued research in this area. Further investigation of the particular system described in this report is warranted because minimum distance braking is provided without skid; whereas, typical anti-skid schemes merely prevent skid by releasing the brake on any wheel approaching wheel lock-up which most likely sacrifices significant braking distance.

Further research into mu-slip characteristics between tire and pavement is necessary. Such research should provide a clear understanding of the basic physical phenomena occurring between tire and pavement. Such understanding should be substantiated by accurate experimental measurements, where all assumptions are properly validated by calibrated measurements.

### ACKNOWLEDGEMENTS

The principal investigator would like to acknowledge the assistance of the contract monitor, Dr. Richard Campbell of NASA-MSFC, who contributed many ideas during numerous discussions. Mr. Edmund C. Wiggins, research assistant at UMR, served as programmer and devised the three dimensional plotting scheme for presentation of the simulation results. Dr. Hugh F. Spence, computer engineer at UMR, contributed helpful suggestions during many in-house discussions of the contract work.

## ADAPTIVE BRAKING SYSTEM

### Introduction

This report presents a new approach to the problem of braking a vehicle in minimum distance. To brake in minimum distance, the tire slip must be controlled to ride the peak of the  $\mu$ -slip curve so that maximum ground force is developed between tire and pavement. The resulting control system differs from anti-skid systems which merely react to impending wheel lockup.

In Part I, a simplified model is presented to permit development of a sound control strategy. Lyapunov techniques are used to derive a peak-riding adaptive controller applicable to each wheel of a braking vehicle.

In Part II, the controller is applied to a more sophisticated model of a braking airplane with strut bending dynamics included. Simulation results verify the peak-riding property of the controller and the rapid adaption of the controller to extreme runway conditions (i.e., wet-dry-wet).

In Part III, practical considerations are discussed including the effect of actuator dynamics, perturbation frequency, type and location of sensors, absence of a free wheel, and a method in which the pilot's braking commands can be interfaced with the peak riding system.



# I. Development of A Peak Riding Adaptive Controller.

## Simplified Model

Consider the problem of braking a vehicle which is moving on a single wheel along the earth's surface by applying a torque to the rolling wheel (see Figure 1). Equations of motion for this simplified model (neglecting rotational dynamics of the mass) are

$$\dot{v} = -f/M \quad (1)$$

$$\dot{\omega} = fR/I - T/I. \quad (2)$$

The ground force  $f$  is related to the coefficient of friction between the tire and pavement  $\mu$  and the weight of the vehicle by

$$f = \mu gM. \quad (3)$$

However, studies have indicated that  $\mu$  depends not only on surface conditions (i.e., dry, wet), but also upon the relative velocity between the tire and pavement, or slip-velocity,  $y$ , given by:

$$y = v - \omega R. \quad (4)$$

Typical curves for  $\mu$  vs.  $y$  are given in Figure 2. Although various experimental measurements of  $\mu$ -slip curves have produced many different shape curves, it is generally agreed that for most surface conditions and rolling velocities, the peak value of  $\mu$  occurs at some non-zero slip velocity and that higher slip velocities will result in decreased  $\mu$  (i.e., the negative slope region of curve does indeed exist). The slip at which the peak  $\mu$  occurs is referred to as the point of incipient skid,  $y_p$ .

To achieve minimum distance braking, maximum deceleration of the vehicle, which is synonymous with peak  $\mu$ , must be obtained. Thus, slip velocity must be controlled in some manner that causes

peak  $\mu$  to be developed between tire and pavement. The slip controller must necessarily be adaptive and self-optimizing since neither  $\mu$  nor  $y_p$  are known. Furthermore,  $\mu_p$  and  $y_p$  are dependent upon surface conditions, temperature, tire inflation, etc., and thus can be expected to vary throughout any particular braking trajectory.

### Slip Controller

To examine the problem of controlling slip velocity, equations (1) through (3) can be substituted into the derivative of (4) to obtain

$$\dot{y} = -a\mu(y) + \beta \quad (5)$$

where

$$a = g(1 + \frac{MR^2}{I}) \text{ and } \beta = RT / I.$$

Equation (5) can be considered a first-order process with nonlinear feedback. The control input  $\beta$  must be constrained such that  $\beta \geq 0$  when the wheel is rotating in the positive direction since conventional brakes can only decelerate the wheel and hence increase slip-velocity. This dynamic process is pictured in Figure 3.

Since  $y$  must be controlled in order to ride the peak of the  $\mu$ - $y$  curve, let us first design a controller which will keep  $y$  arbitrarily close to some set point  $\gamma$ . Using Lyapunov design techniques, an appropriate Lyapunov function is:

$$V = \frac{1}{2} (\gamma - y)^2 \quad (6)$$

If  $\gamma$  is constant, then (5) into the derivative of (6) produces

$$\dot{V} = (\gamma - y) (a\mu - \beta). \quad (7)$$

Now can  $\beta$  be chosen so that  $\dot{V}$  is negative definite in  $(\gamma - y)$ ? A

first attempt may be to choose  $\beta$  large in magnitude, so that it overrides the  $a\mu$  term, and identical in sign to  $\gamma - y$ . In light of this, along with the constraint  $\beta \geq 0$ , a choice which deserves further analysis is:

$$\beta = \begin{cases} 0 & \text{for } y > \gamma \\ G(\gamma - y) & \text{for } y \leq \gamma \end{cases}. \quad (8)$$

Equation (8) into (7) provides:

$$\dot{y} = \begin{cases} a\mu(\gamma - y) < 0 & \text{for } y > \gamma \\ -(\gamma - y) [G(\gamma - y) - a\mu] & \begin{cases} > 0 & \text{for } \gamma - \frac{a\mu}{G} < y < \gamma \\ < 0 & \text{for } y < \gamma - \frac{a\mu}{G} \end{cases} \end{cases}. \quad (9)$$

From (9), we can conclude that  $y$  approaches one of two equilibrium points: either  $y = \gamma$  or  $\gamma - \frac{a\mu}{G}$ , as shown in Figure 4. Actually, these two points can be made arbitrarily close by choosing  $G \gg a\mu$ . Thus, if  $\gamma$  is the set point for slip velocity, then  $y$  will converge arbitrarily close to  $\gamma$ .

### Peak-Riding Controller

If the  $\mu$ -slip curve of Figure 2a is differentiated with respect to  $y$ , as shown in Figure 5, then clearly  $y$  must be adjusted according to the sign of  $\partial\mu/\partial y$  in order that  $y_p$  be reached. Since  $\gamma$  is the setpoint for  $y$ , we can choose  $\text{sgn } \dot{\gamma} = \text{sgn } \partial\mu/\partial y$  thus assuring that  $\gamma$  approaches a value which forces  $\partial\mu/\partial y = 0$  or  $y = y_p$ .

Unfortunately, the sign of  $\partial\mu/\partial y$  is not known, nor is  $y_p$ . However, so long as  $\dot{y} \neq 0$  (i.e., slip velocity is not constant), the sign of  $\partial\mu/\partial y$  can be obtained from  $\dot{\mu}$  and  $\dot{y}$ . Under the assumption

that the mu-slip curve is stationary (i.e.,  $\partial\mu/\partial t = 0$ ):

$$\dot{\mu} = \frac{\partial\mu}{\partial y} \dot{y}. \quad (10)$$

Multiplying (10) by  $\dot{y}$  and equating signs gives:

$$\text{sgn } \ddot{\mu} y = \text{sgn } \frac{\partial\mu}{\partial y} \text{ for } \dot{y} \neq 0. \quad (11)$$

Thus,  $\gamma$  can be automatically adjusted to force  $y$  closer to  $y_p$  by:

$$\dot{\gamma} = K\ddot{\mu} y. \quad (12)$$

Actually,  $\dot{\mu}$  and  $\dot{y}$  are not available. However, approximate derivative filters used on measured signals should provide satisfactory results since only the signs of the estimated derivatives need be accurate for correct adjustment.

The convergence of  $\gamma$  to the desired value requires  $\dot{y} \neq 0$ , which can be implemented by adding a small perturbation signal  $\delta$  to (8)

$$\beta = \begin{cases} 0 & \text{for } y > \gamma + \delta \\ G(\gamma - y + \delta) & \text{for } y < \gamma + \delta \end{cases},$$

(8)\*

## II. Application With Simulation Results.

### Braking Airplane Model

The results of the previous section will now be applied to a model of a braking airplane similar to that of Figure 1 except that strut bending dynamics are included in the model shown in Figure 6. Equations of motion are:

$$\dot{v} = -g\mu(y) \quad (13)$$

$$I\dot{\omega} = MgR \mu(y) - T \quad (14)$$

$$M_s \ddot{z} + C_s \dot{z} + K_s z = Mg\mu(y) + K_T T \quad (15)$$

$$y = v - R\omega - \dot{z}, \quad (16)$$

where  $z$  is the strut horizontal displacement due to cantilever bending caused by ground force  $f$  and brake torque  $T$ .  $M_s$ ,  $C_s$ ,  $K_s$ , and  $K_T$  are strut parameters [1], while all other symbols retain their previous definitions. Brake torque  $T$  is assumed to be proportional to brake pressure  $P$  and must oppose the rotation  $\omega$ . With the sign convention of Figure 6, we can let:

$$T = (K_b \operatorname{sgn} \omega) P \quad (17)$$

where brake pressure is now the control input for braking the airplane.

### Controller

Analogous to equation (8)\* and (12), the controller is defined as

$$P = G(\gamma - y + \delta), \quad 0 \leq P \leq P_{\max} \quad (18)$$

$$\dot{\gamma} = K\hat{\mu}\hat{y}, \quad 0 \leq \gamma \leq \gamma_{\max} \quad (19)$$

where  $\hat{\mu}$  and  $\hat{y}$  are estimates of  $\mu$  and  $y$  derived from the following filters

C

$$\dot{\hat{\mu}} = K_{\mu} (\mu - \hat{\mu}) \quad (20)$$

$$\dot{\hat{y}} = K_y (y - \hat{y}) \quad (21)$$

The Gains on  $\dot{\hat{\mu}}$  and  $\dot{\hat{y}}$  can be limited before entering equation (19) which in turn bounds  $\dot{\gamma}$ . Bounding  $\dot{\gamma}$  has no theoretical significance, since only the sign of  $\ddot{\mu y}$  is important.

Brake pressure, from a practical viewpoint, must be held between limits such as those specified in (18). Similarly,  $\gamma$  should be held between the limits specified in (19). The lower limit on  $\gamma$  is advisable since the peak  $\mu$  will always fall to the right of  $y = 0$ . The upper limit  $\gamma_{\max}$  can be chosen to prevent excessive slip-velocity and consequently tire wear in the event that a peak  $\mu$  does not exist or is far to the right on the  $\mu$ -slip curve. Essentially,  $\gamma_{\max}$  prevents the system from operating in the region  $y > \gamma_{\max}$  except for brief transients at touch down.

### Simulation Results

A simulation diagram of equations (13) through (21) is shown in Figure 7. A detailed analog computer diagram, complete with scaling information, is shown in Appendix A. Note that two  $\mu$ -slip curves are available, one simulating dry pavement conditions and the other wet.

Time histories of  $\mu$ -slip for an elapsed time of 0.8 seconds from touch down are shown in Figures 8 and 9. In Figure 8, the system operates on wet pavement for the first 0.4 seconds at which

time an abrupt change to dry pavement occurs. The wheel velocity is zero at touch down, hence operation begins at full slip velocity in the lower right-hand corner of Figure 8. In Figure 9, the dry pavement is encountered first, followed by the wet pavement 0.4 seconds after touch down. Note that the time axis is reversed on Figure 9 and that the trajectory begins in the upper right-hand corner. Examination of these figures shows the excellent peak riding capabilities of this system, together with rapid adaption to sudden change in pavement conditions. Table 1 specifies all parameter values used in the simulation.

$g = 32.2 \text{ ft/sec}^2$ $Mg = 10,000 \text{ lbs}$ $R = 1 \text{ ft}$ $I = 2 \text{ lb-ft-sec}^2$	accel of gravity wt of airplane tire radius tire inertia	Rigid Body Parameters
$M_s = 10 \text{ lb-sec}^2/\text{ft}$ $C_s = 98 \text{ lb-sec/ft}$ $K_s = 6,000 \text{ lbs/ft}$ $K_T = .15 \text{ ft}^{-1}$	strut mass strut damping strut spring constant	Strut Parameters
$\mu_{p \text{ dry}} = 0.85$ $\mu_{p \text{ wet}} = 0.24$ $y_{p \text{ dry}} = 12 \text{ ft/sec}$ $y_{p \text{ wet}} = 37 \text{ ft/sec}$	peak $\mu$ peak $\mu$ slip velocity at $\mu_p$ slip velocity at $\mu_p$	Mu-slip Curve Data
$a_p = 2.5 \text{ ft/sec}$ $t_p = 12.5 \text{ msec}$	perturbation amplitude perturbation period (80 hz freq)	Perturbation Signal
$K_b = 1 \text{ ft}^3$ $G = 3,000 \text{ lb-sec/ft}^3$ $P_{\max} = 20,000 \text{ lbs/ft}^2$ $K = 0.4 \text{ sec}$ $\gamma_{\max} = 60 \text{ ft/sec}$	torque/pressure brake constant pressure/velocity controller gain pressure limit peak-riding adaption gain slip-velocity limit	Controller Parameters
$K_{\dot{\mu}} = 5,000 \text{ sec}^{-1}$ $\dot{\mu} \text{ limit} = 15 \text{ sec}^{-1}$ $K_{\dot{y}} = 500 \text{ sec}^{-1}$ $\dot{y} \text{ limit} = 1500 \text{ ft/sec}^2$		Filter Parameters

Table 1. Parameter Values For Simulation of Braking Airplane



### III. Practical Considerations

#### Measurement of $y$

Realization of the controller of Figure 7 requires measurement of  $y$  and  $\mu$ . Actually,  $y$  can be computed from measurement of  $\omega$ ,  $v$ , and  $\dot{z}$ . This leads to a fairly complicated set of sensors. Wheel speed is easily measured by some type of tachometer. Vehicle velocity can be established by measurement of a free-wheel speed. On an automobile, this would require the addition of an expensive free wheel; but on an airplane, a nose wheel could be used as a free wheel. Including  $\dot{z}$  in the computation of  $y$  produces further difficulties. If the free wheel is placed on the strut, then  $v - \dot{z}$  can be measured as a single wheel speed. If not,  $\dot{z}$  must be estimated by other means, any of which would probably be expensive.

To alleviate this problem, let us examine how  $y$  is used by the controller in search for alternate measurements which might yield a more practical solution. First,  $y$  is used to drive the  $\hat{y}$  filter. Actually, all that is needed here is a signal which is changing in the same direction as  $y$ . Almost all rapid changes in  $y$  are due to changes in wheel speed  $\omega$ . This is especially true if the perturbation frequency is chosen well above the resonant frequency of the strut so that the strut does not respond to the perturbations. Hence  $-\omega$  can be used in place of  $y$  for the  $\hat{y}$  filter.

Secondly,  $y$  is used in comparison to  $\gamma$  for brake pressure actuation. Here again, wheel speed could be used, but  $\gamma$  then must be the set point for wheel speed which produces peak- $\mu$ . Our argument for limiting slip-velocity in extreme situations by the

$\gamma_{\max}$  setting now fails. To correct this situation, an estimated velocity  $v$  could be used along with  $\omega$  to provide the actuator signal. Inaccurate measurement of  $v$  (i.e., a slowly varying bias) should not degrade performance since the adaptive controller would respond to this as it would to a slowly varying  $y_p$  on the mu-slip curve. An initial  $v$  could be established from wheel speed prior to actuation of brake pressure. This could be integrated downward by a deceleration measurement or proportional  $\hat{\mu}$  which is an average developed  $\mu$ . Of course on an airplane, the free nose wheel speed could be used for  $v$ .

The above ideas were tested on the previous simulation and no significant degradation in performance was noted.

#### Measurement of $\mu$

The measurement of  $\mu$  for the  $\hat{\mu}$  filter poses somewhat of a practical problem since a signal is needed for each braking wheel in order that each wheel ride the peak of its mu-slip curve. However, a calibrated measurement is not necessary since the measured signal needs only to change with changing  $\mu$ , that is, a slowly varying bias is again insignificant. Since the developed ground force must be transmitted to the vehicle through the wheel bearing, it may be feasible to mount a pair of strain gauges near the bearing, positioned so that vertical forces transmitted by the bearing to the vehicle are cancelled while horizontal forces are cumulative. Although this idea has not been tested, it is believed that experimentation is warranted.

Figure 10 portrays the strain gauge configuration for both (a) a wheel rotating with an axle such as the rear wheels of an automobile and (b) a wheel rotating on a stud such as the front wheels of an automobile. Strain gauges A and B are strained in opposite directions for a horizontal force and in the same direction for a vertical force. Thus, a horizontal force will unbalance the bridge, while a vertical force will not unbalance the bridge.

### Actuator Dynamics

Equation (18) implies that brake pressure can be varied algebraically, with the input signal  $(\gamma - y + \delta)$ . To study the effect of some lag between actuator input and developed brake pressure, the following first order actuator was tested in the simulation:

$$\dot{P} = -bP + bG(\gamma - y + \delta), \quad 0 \leq P \leq P_{\max} \quad (22)$$

Figures 11 and 12 show the effect of this actuator lag for  $b = 500$  and  $b = 50$ , respectively. These correspond to actuator rolloff frequencies of about 80 hz and 8 hz. As expected, the sluggishness of the actuator certainly downgrades peak riding performance by greatly increasing the magnitude of slip oscillation about  $y_p$ .

The degradation in performance caused by the sluggish actuator can be largely overcome by feedforward around the  $\gamma$  integrator. This gives the actuator lead information about  $\gamma$ , enabling the actuator-set point combination to respond more quickly. Figure 13 is a repeat of Figure 12, except that the actuator input is  $(\gamma - y + \delta + 0.005\dot{\gamma})$ .

### Interface With Pilot or Driver

The adaptive braking system is easily interfaced with conventional operator controls, such as a foot pedal. If  $P_{\max}$ , the limit

on brake pressure, is taken as the operator's input, then peak riding will occur only when excessive input is applied.

For example, suppose the operator applies enough pedal pressure to produce rapid, but not maximum deceleration on dry pavement. The controller will operate to the left of the peak as shown in Figure 14. If wet pavement were encountered, the wheels would lock. However, the adaptive controller automatically rides the peak of the wet mu-slip curve. Figure 14 illustrates the dry-to-wet and wet-to-dry transitions when the operator commands an average deceleration.

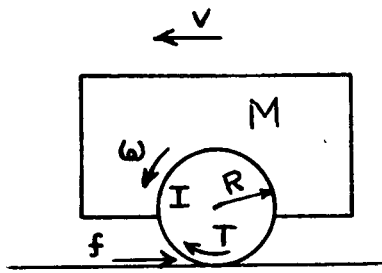
## Conclusions

A peak-riding adaptive controller for minimum distance braking has been described. Each wheel is controlled independently and rides the peak of its mu-slip curve. Simulations show that the controller operates as predicted by the theoretical derivation.

Although development work must be done to perfect a practical system, the controller presented here is applicable to any land vehicle which uses wheel braking for deceleration of the vehicle. With some modification, the controller is compatible with relatively sluggish brake actuators. The controller interfaces easily with conventional braking schemes (i.e. foot-pedal), so that slow decelerations are obtained in the normal manner.

## REFERENCES

1. "Baseline analog simulation for evaluation of brake anti-skid systems", Boeing Document No. D6-58384-3TN. Jan 1969. (36 pages)
2. F. A. BIEHL, "Aircraft landing gear brake squeal and strut chatter investigation", Shock and Vibration Bulletin No. 39 (also Douglas Paper 5240, McDonnell Douglas Corp). (12 pages)
3. H. R. SMITH, "The fifth wheel - a method of adaptive brake control", SAE paper no. 435D. Oct 1961. (9 pages)
4. L. P. GRAYSON, "The status of synthesis using Lyapunov's method", Automatica, vol. 3, pp 91-121. Pergamon Press, 1963.



$M$  mass of vehicle  
 $v$  velocity of vehicle  
 $\omega$  angular velocity of wheel  
 $I$  inertia of wheel  
 $R$  rolling radius of wheel  
 $T$  brake torque applied to wheel  
 $f$  ground force tangential to ground

Figure 1. Simplified braking model.

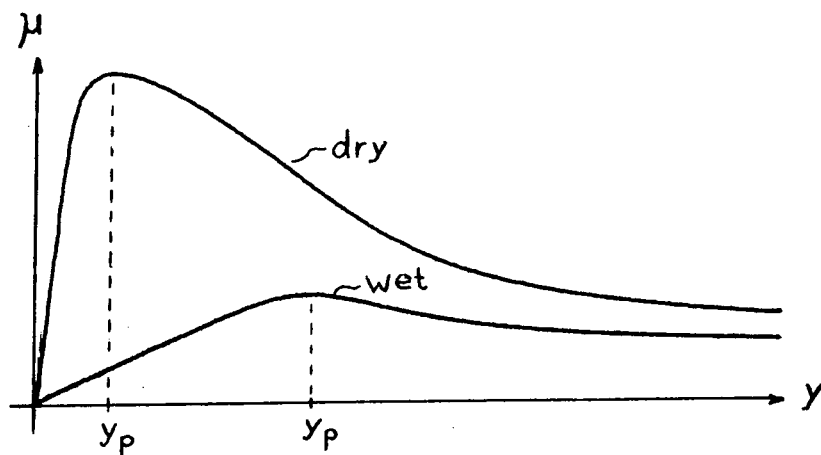


Figure 2. Typical  $\mu$ -slip data for (a) dry pavement.  
 (b) Wet pavement.

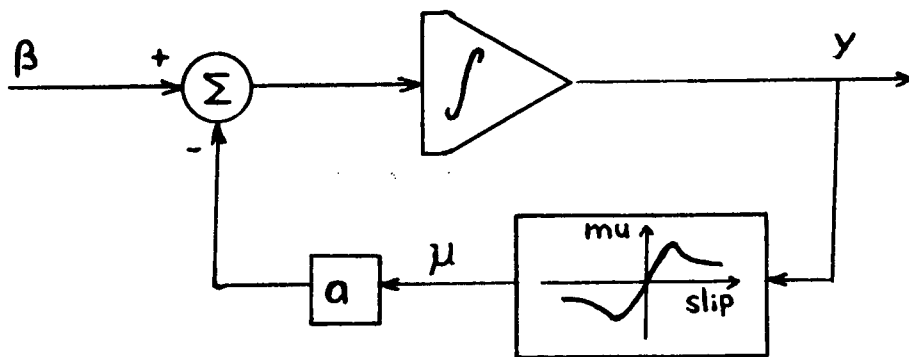


Figure 3. Simplified process for slip-velocity control problem.

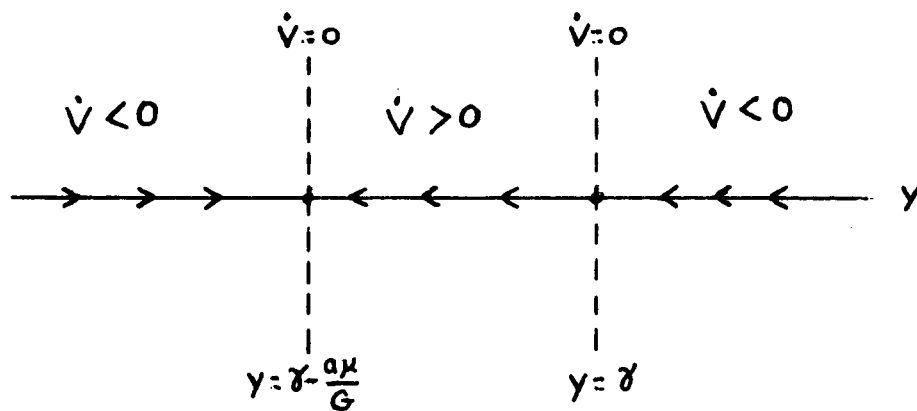


Figure 4. Graphical analysis of equations (6) and (9) with  $\dot{\gamma} = 0$ .



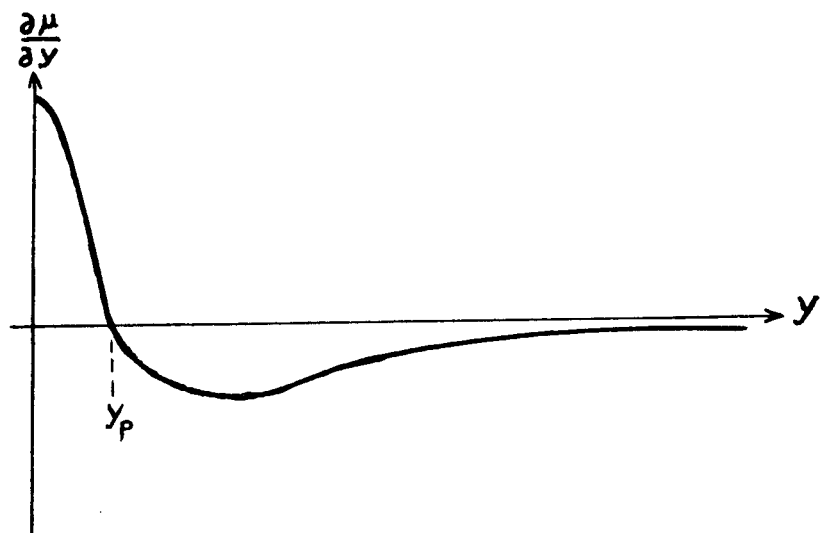


Figure 5. Differentiated mu slip curve.

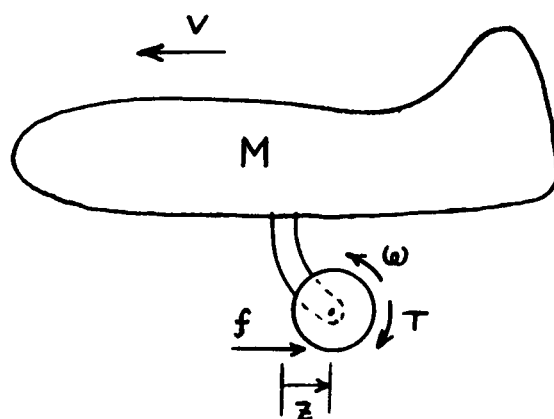


Figure 6. Braking airplane model.

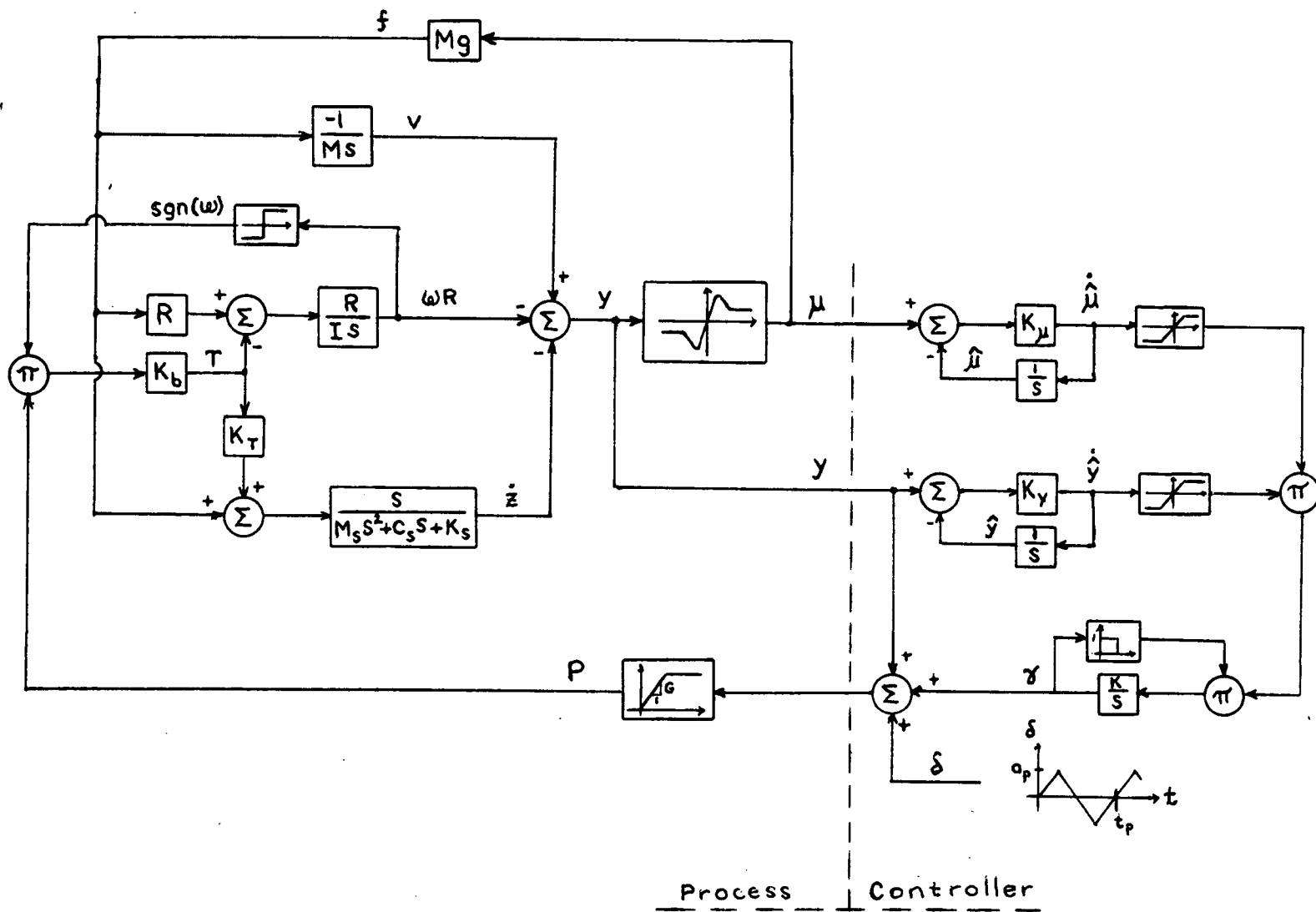


Figure 7. Simulation diagram for the braking airplane.

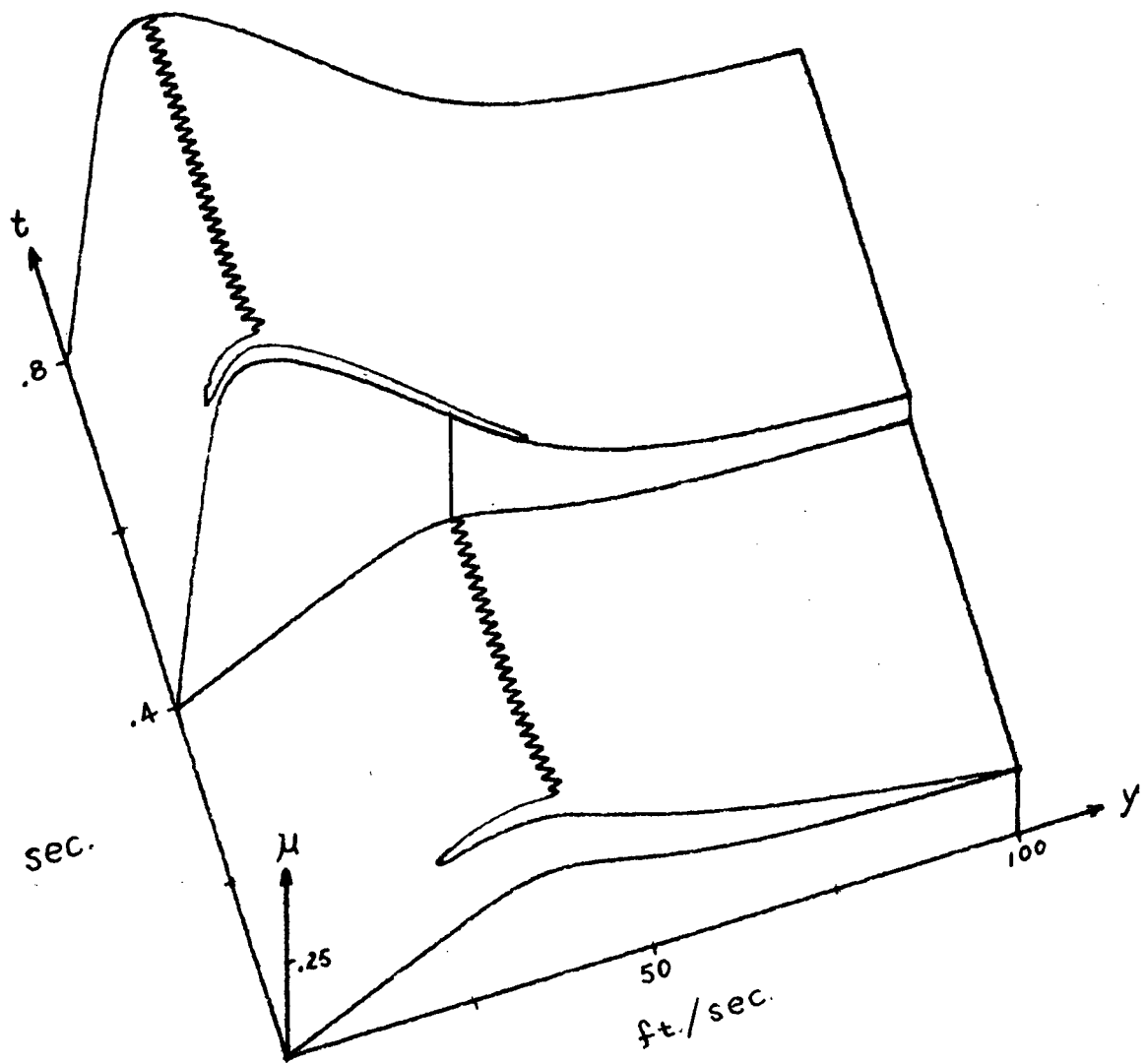


Figure 8. Mu-slip trajectory for wet to dry pavement.

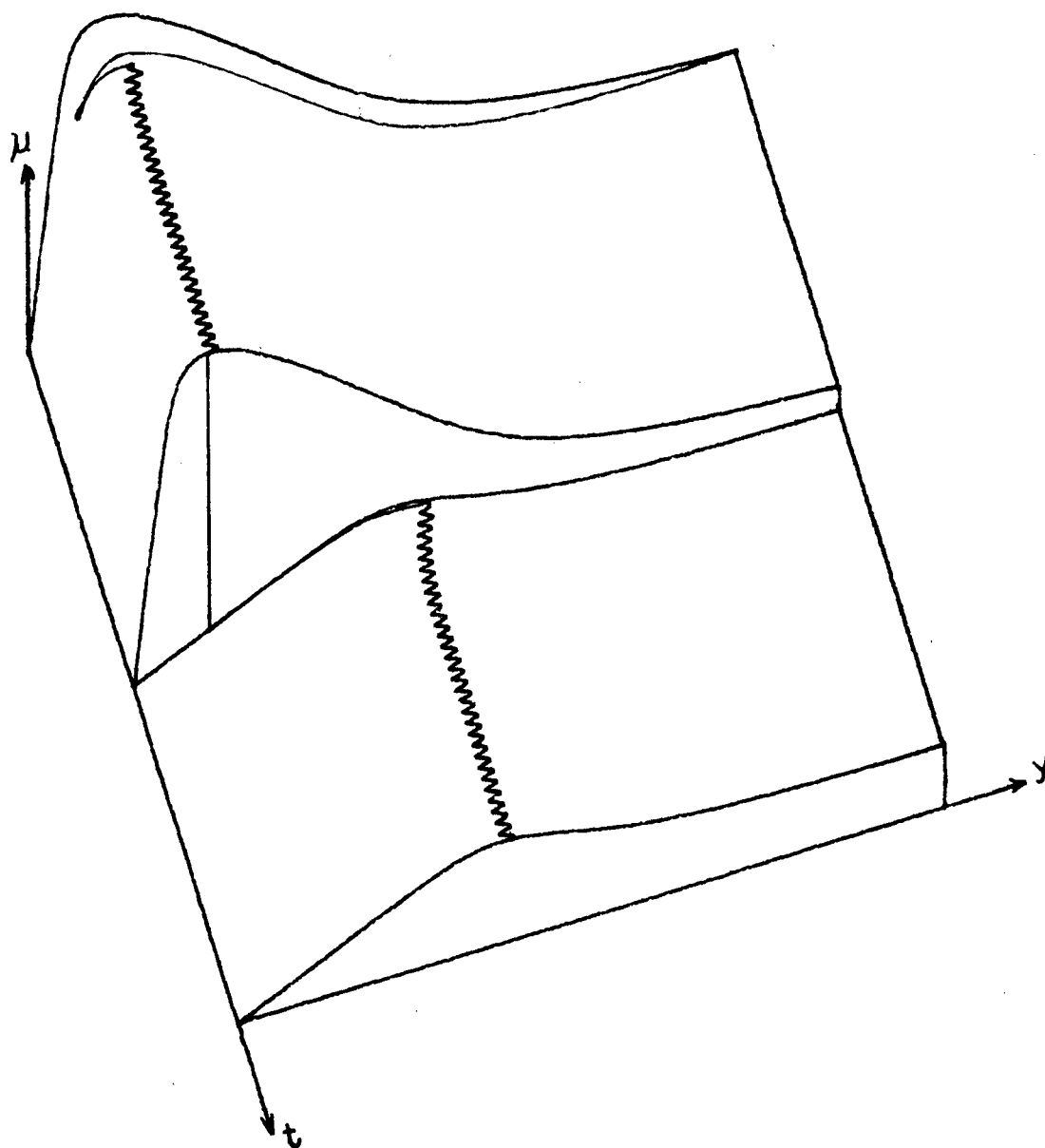


Figure 9. Mu-slip trajectory for dry to wet pavement.

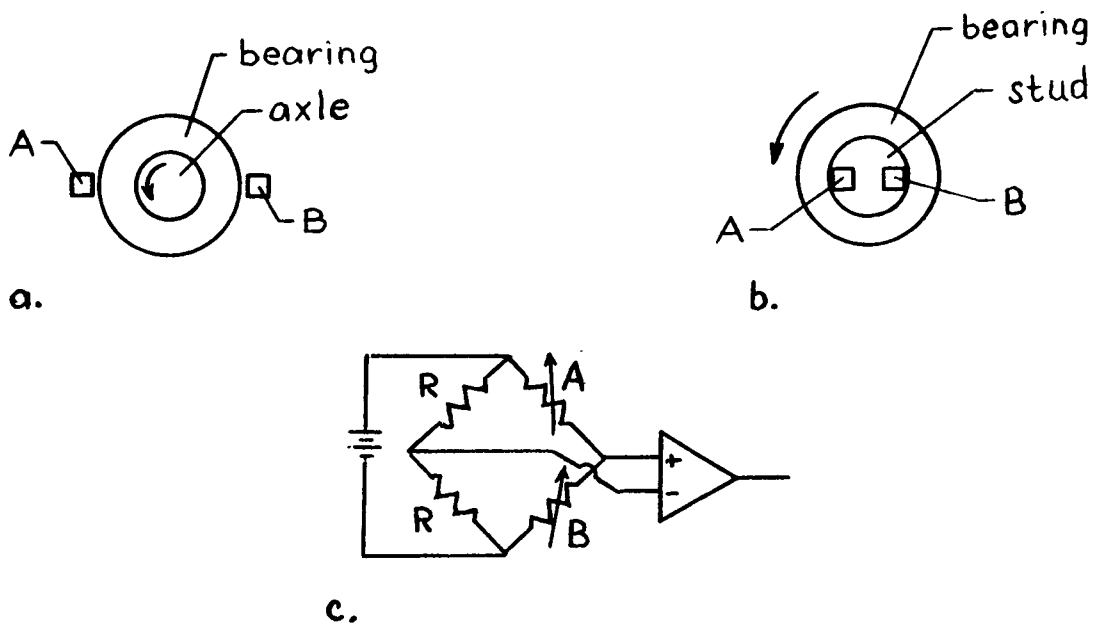


Figure 10. Strain guage sensor configuration A and B.  
(a) Rotating axle. (b) Wheel rotating on stud.  
(c) Bridge and differential amplifier.

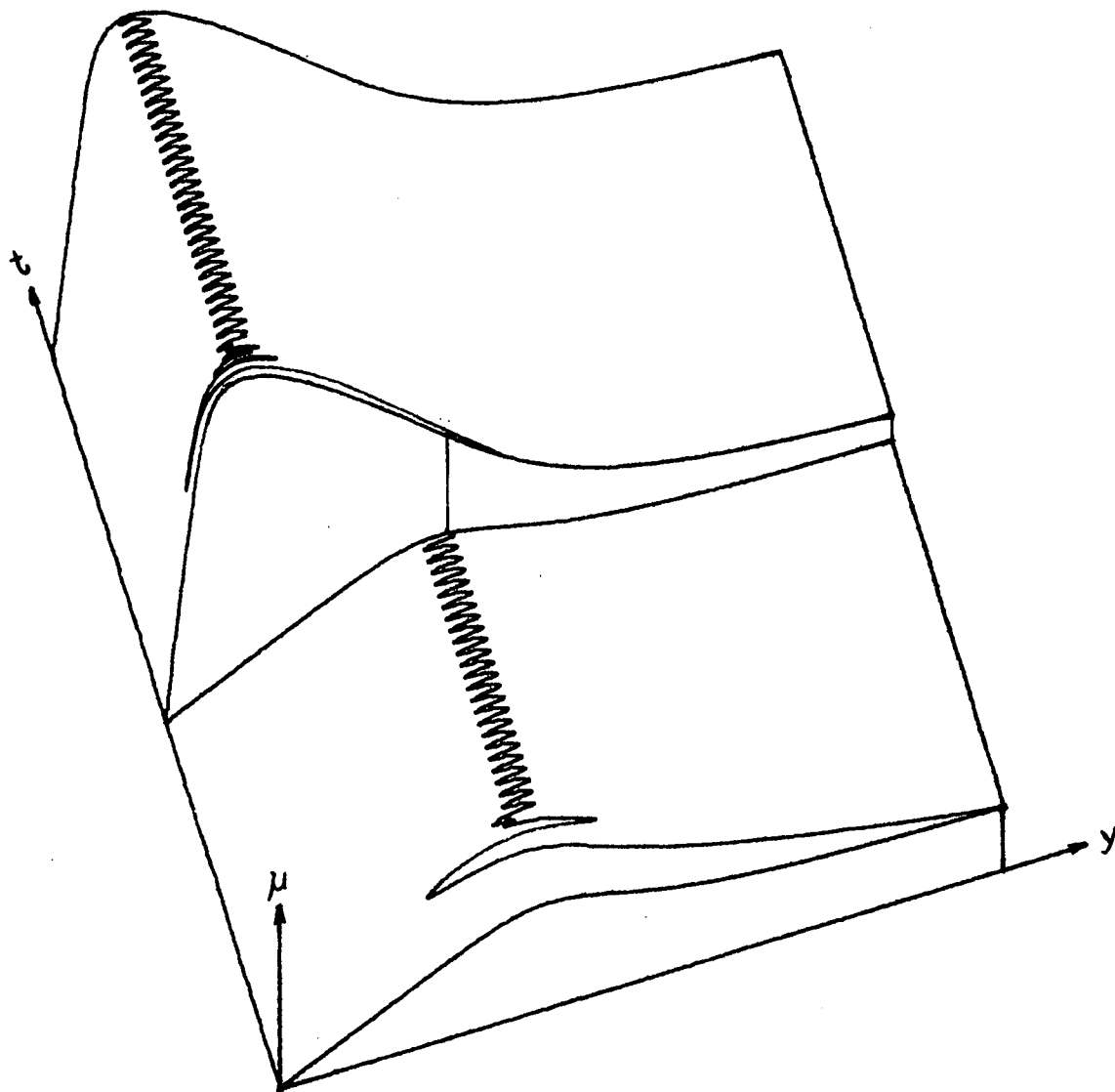


Figure 11. Mu-slip trajectory with 80 hz. actuator.  
(a) Wet to dry pavement.

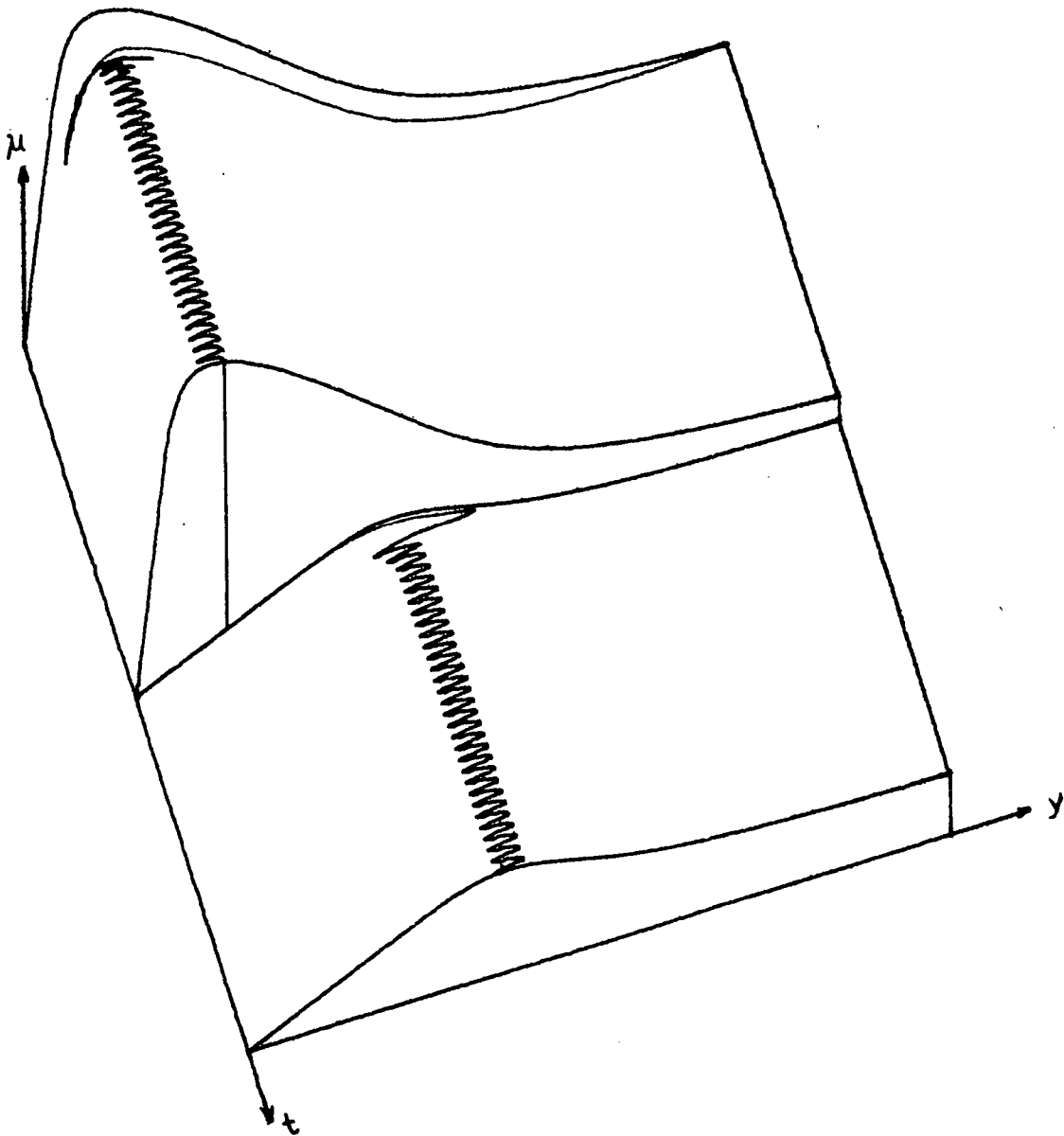


Figure 11. (b) Dry to wet pavement.

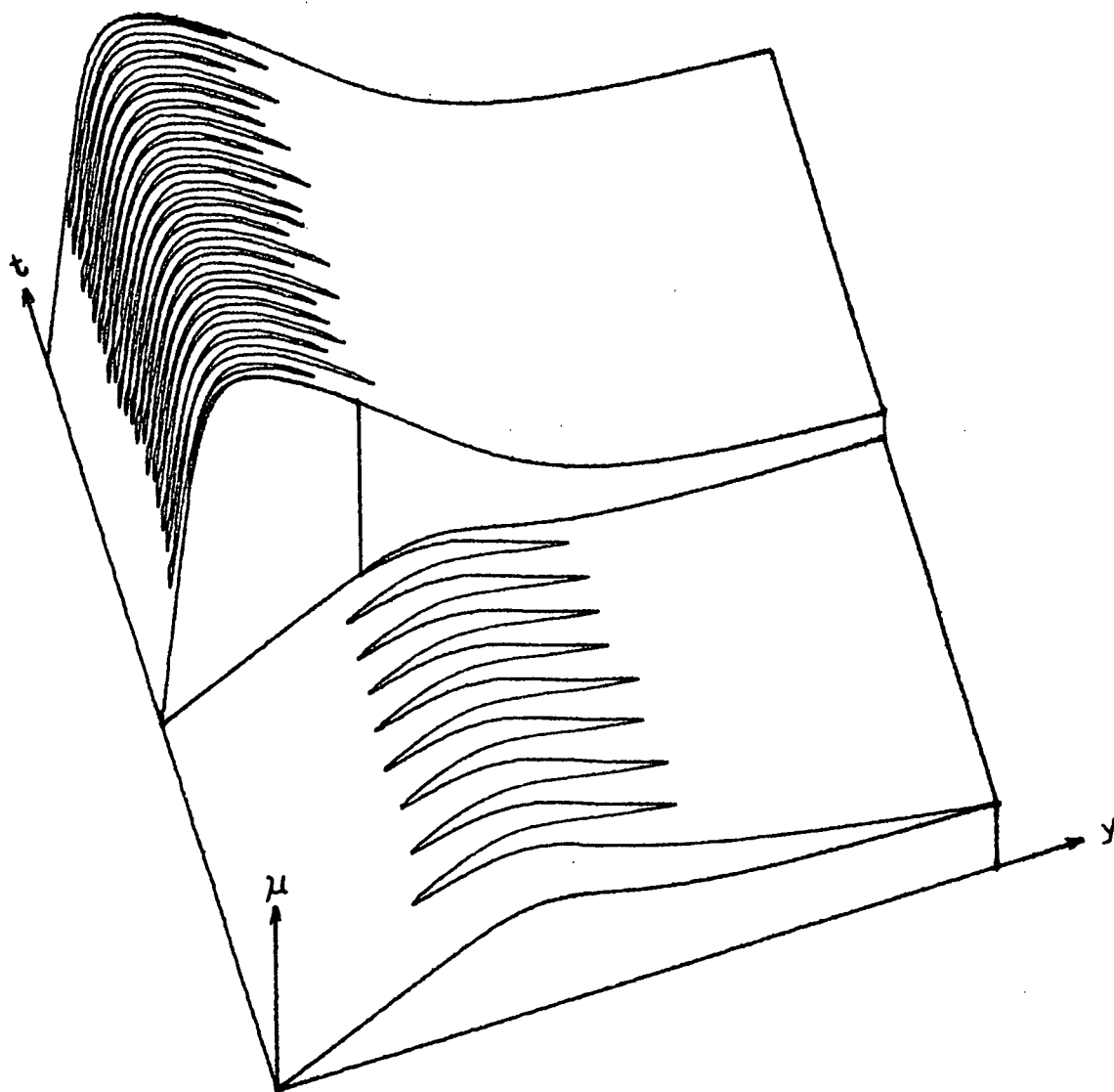


Figure 12. Mu-slip trajectory with 8 hz. actuator.  
(a) Wet to dry pavement.



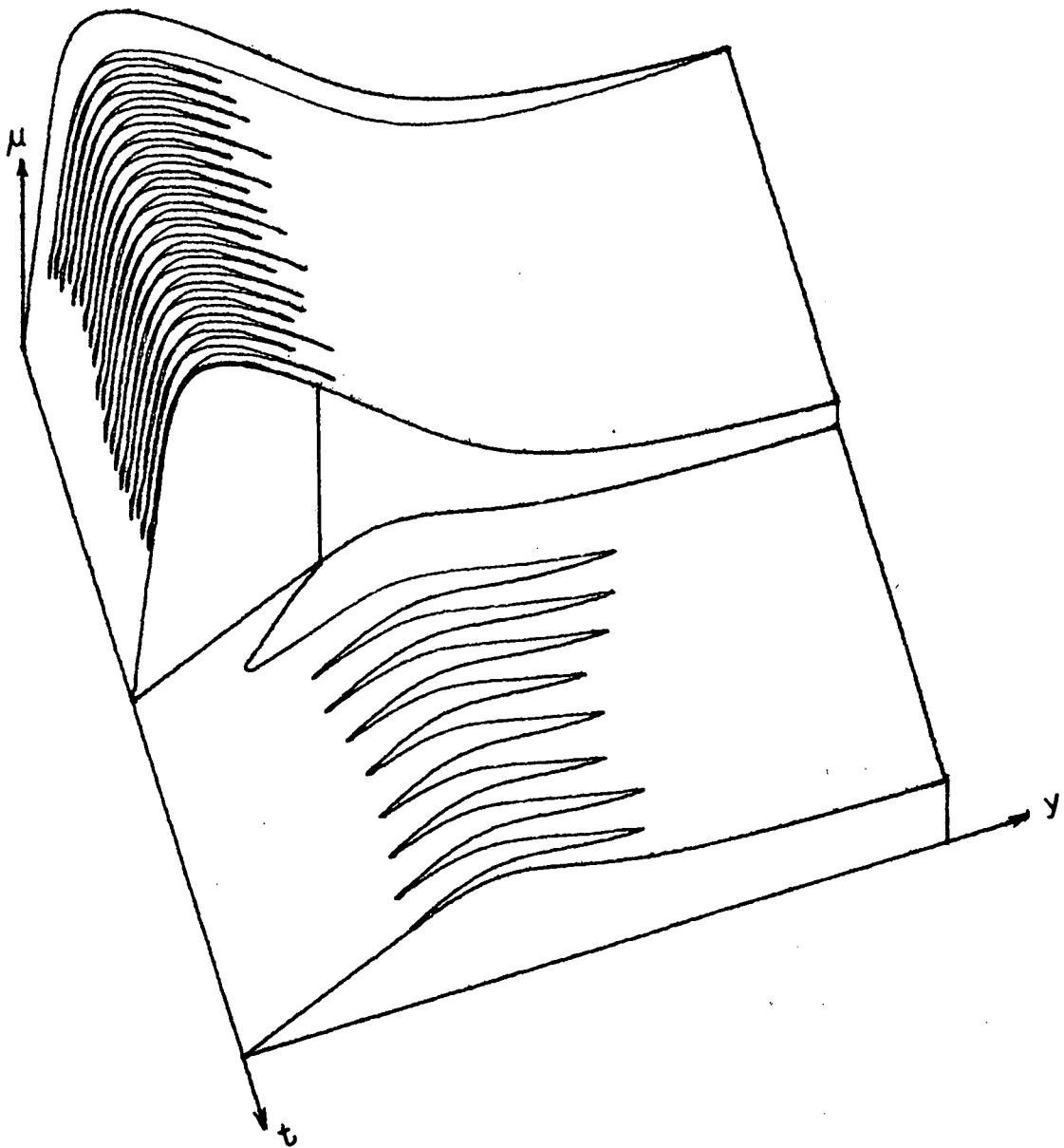


Figure 12. (b) Dry to wet pavement.

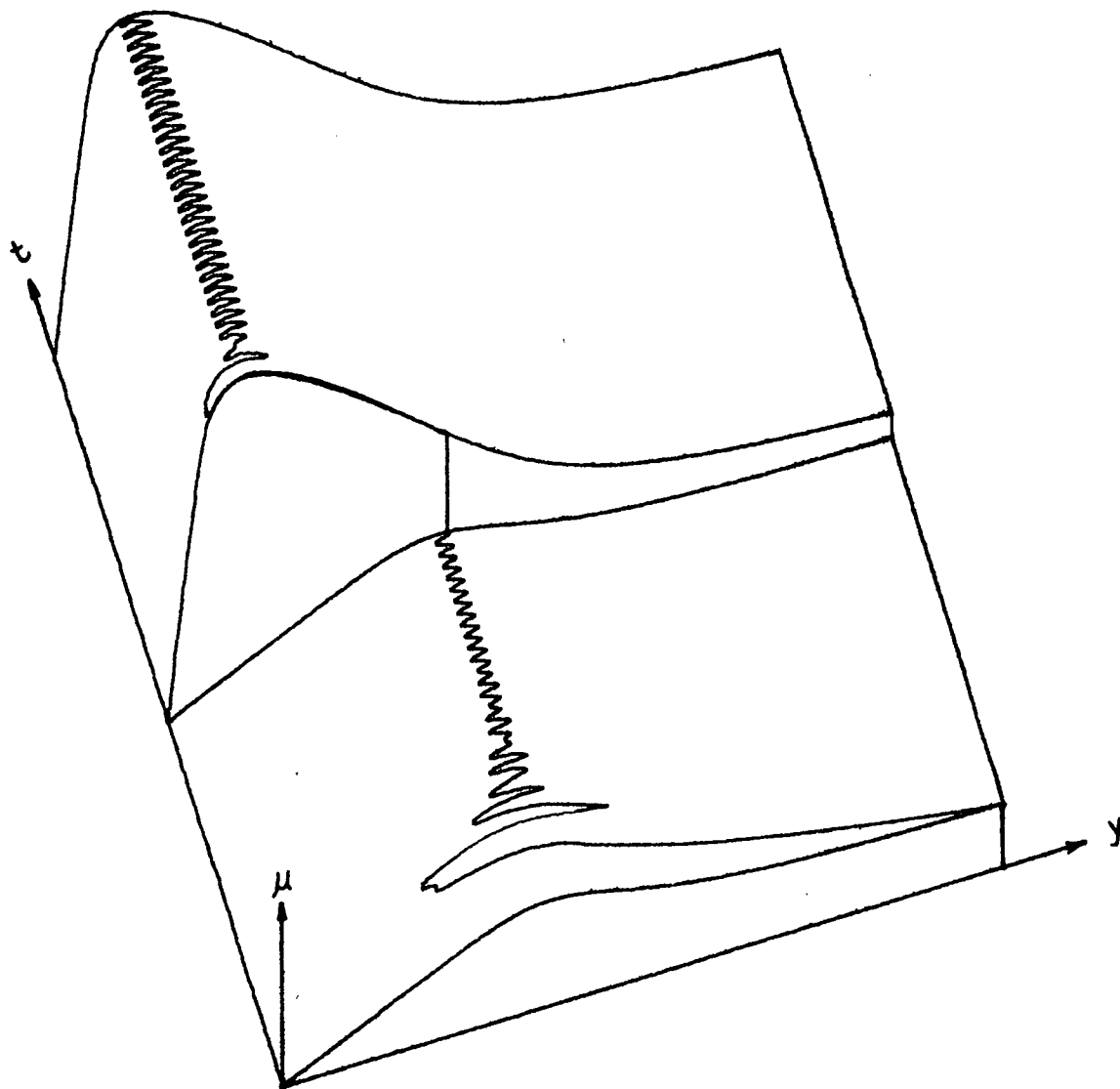


Figure 13. Mu-slip trajectory with 8 hz. actuator and  $0.005 \dot{\gamma}$  feedforward to the actuator. (a) Wet to dry pavement.

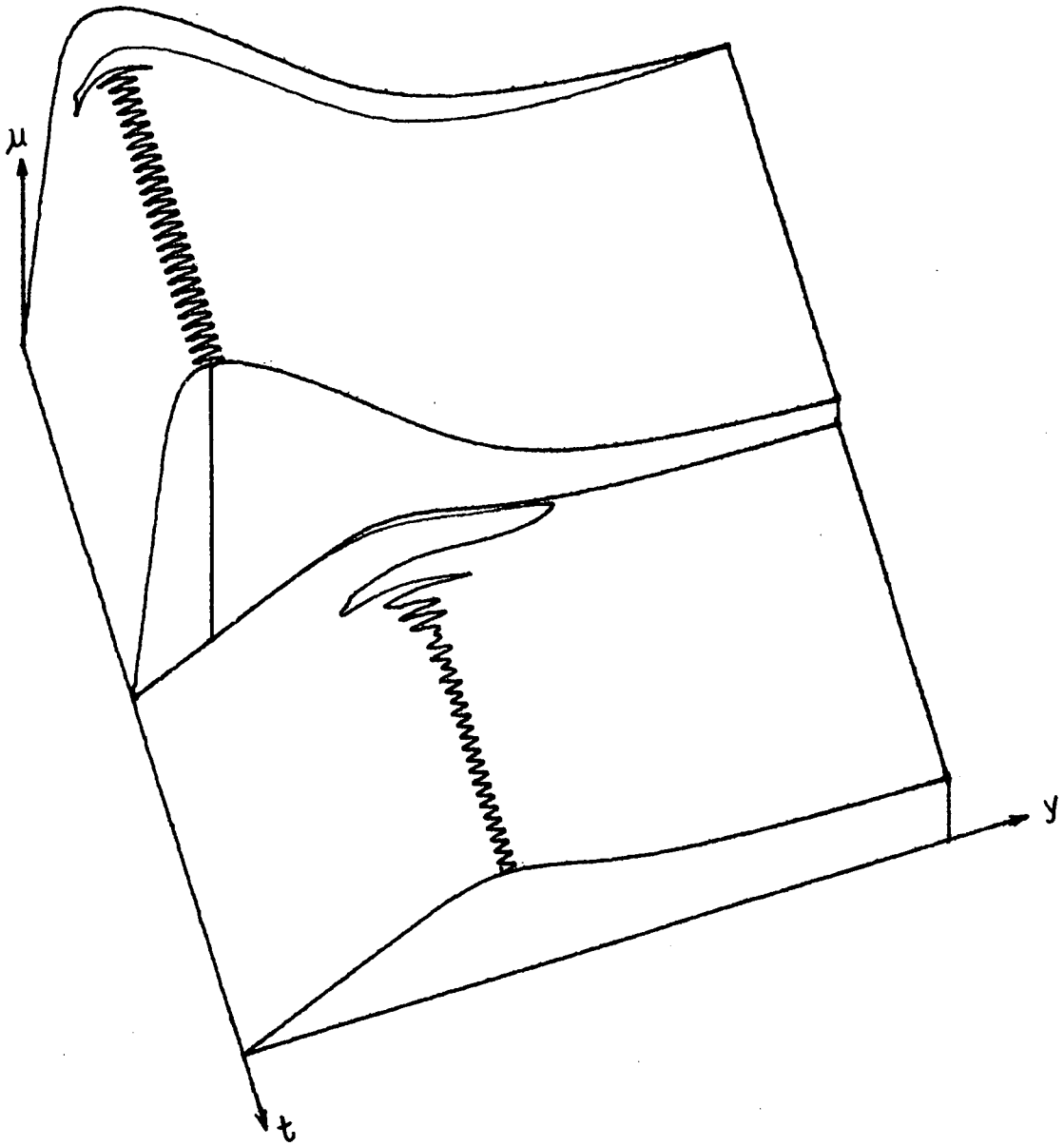


Figure 13. (b) Dry to wet pavement.

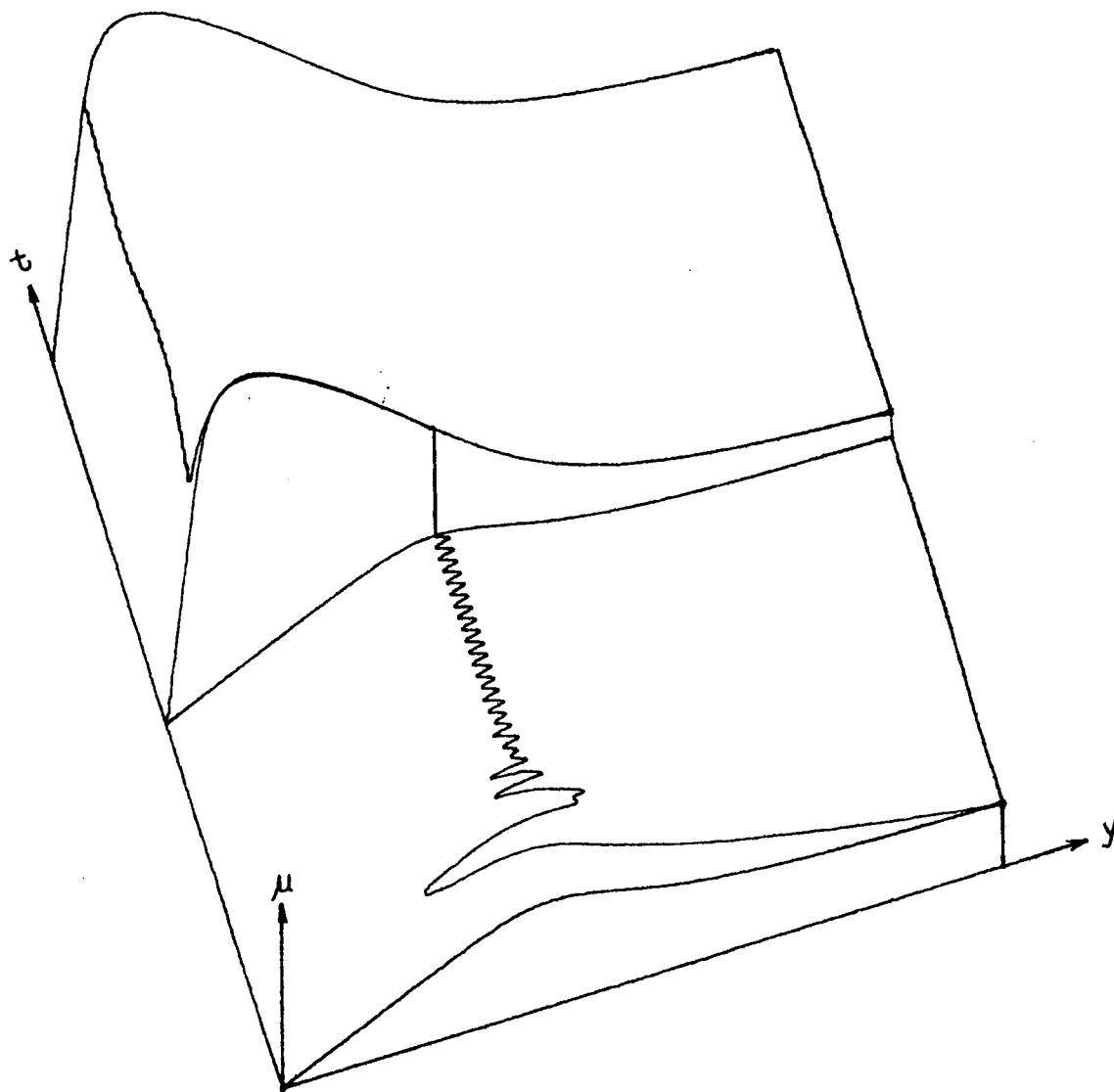


Figure 14. Mu-slip trajectory for less than maximum deceleration commanded by the pilot. (a) Wet to dry pavement.

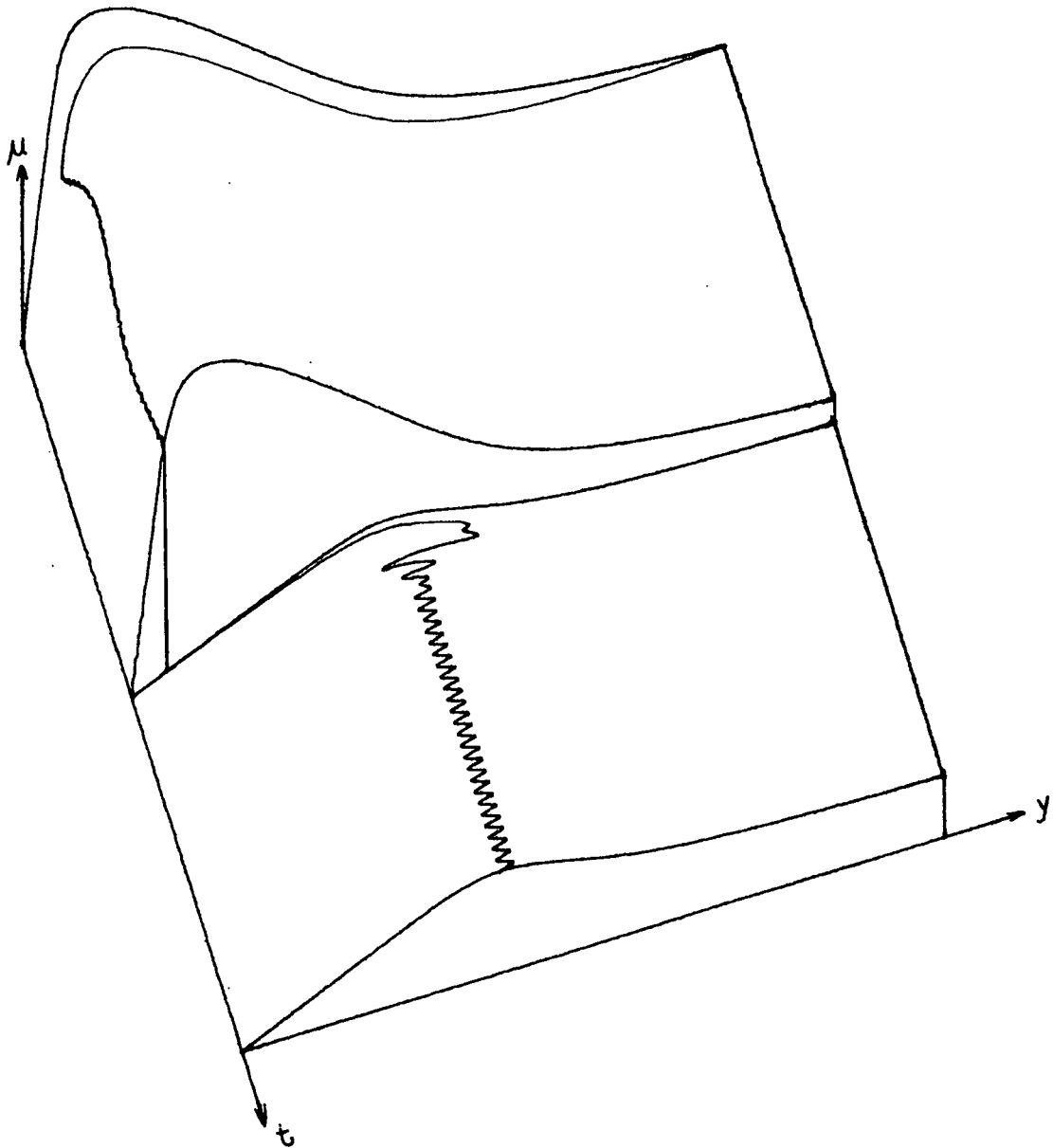


Figure 14. (b) Dry to wet pavement

## APPENDIX A. DETAILS OF ANALOG SIMULATION

The system of Figure 7 with the parameter values in Table 1 was simulated on an EAI TR-48 analog computer. Table 2 defines the symbols used in the computer diagrams of this appendix. Figures A1 through A3 give scaled computer diagrams of the simulation. Integrator gains and potentiometer settings are given in Table 3.

Amplifiers with  $\pm 3$  volt limits were constructed by placing back-to-back 3 volt zener diodes between the output and summing junction of an ordinary amplifier. Other limits were formed with conventional diodes and ungrounded pots.

A time scale factor of 50 was needed to slow responses for plotting on an X-Y recorder. Three dimensional plots were formed by rotating the y and t axes by  $\lambda=17^\circ$ , while holding the u axis vertical. Signals to the X and Y channels of the recorder were:

$$Y = u + t \cos \lambda + y \sin \lambda$$

$$X = y \cos \lambda - t \sin \lambda$$

Axes and mu-slip curves were added to the plots automatically under control of the SCC-650 digital computer which is linked to the TR-48 via the UMR hybrid interface.

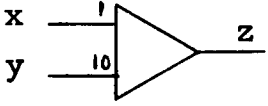
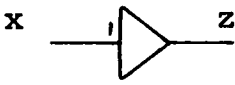
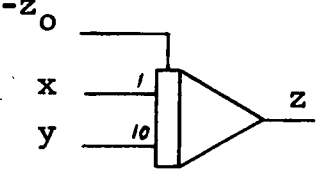
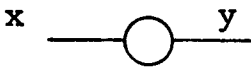
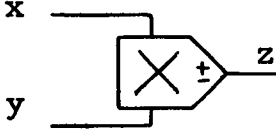
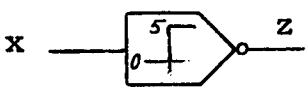
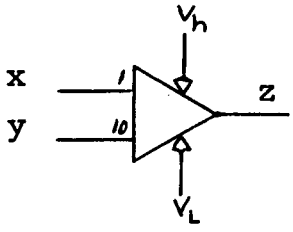
<u>SYMBOL</u>	<u>EXPRESSION</u>	<u>NAME</u>
	$z = -(x + 10y)$	summer (summing amp)
	$z = -x$	sign changer
	$z = -\int_0^t (x + 10y) dt + z_0$	integrator
	$y = \lambda x \quad (0 \leq \lambda \leq 1)$	potentiometer (pot)
	$z = \pm x y / 10$	multiplier
	$z = \begin{cases} 5 & \text{for } x < 0 \\ 0 & \text{for } x > 0 \end{cases}$	comparator
	$z = -(x + 10y) \text{ but } V_L \leq z \leq V_h.$	limited summer

TABLE 2. Symbols used in analog computer diagrams.

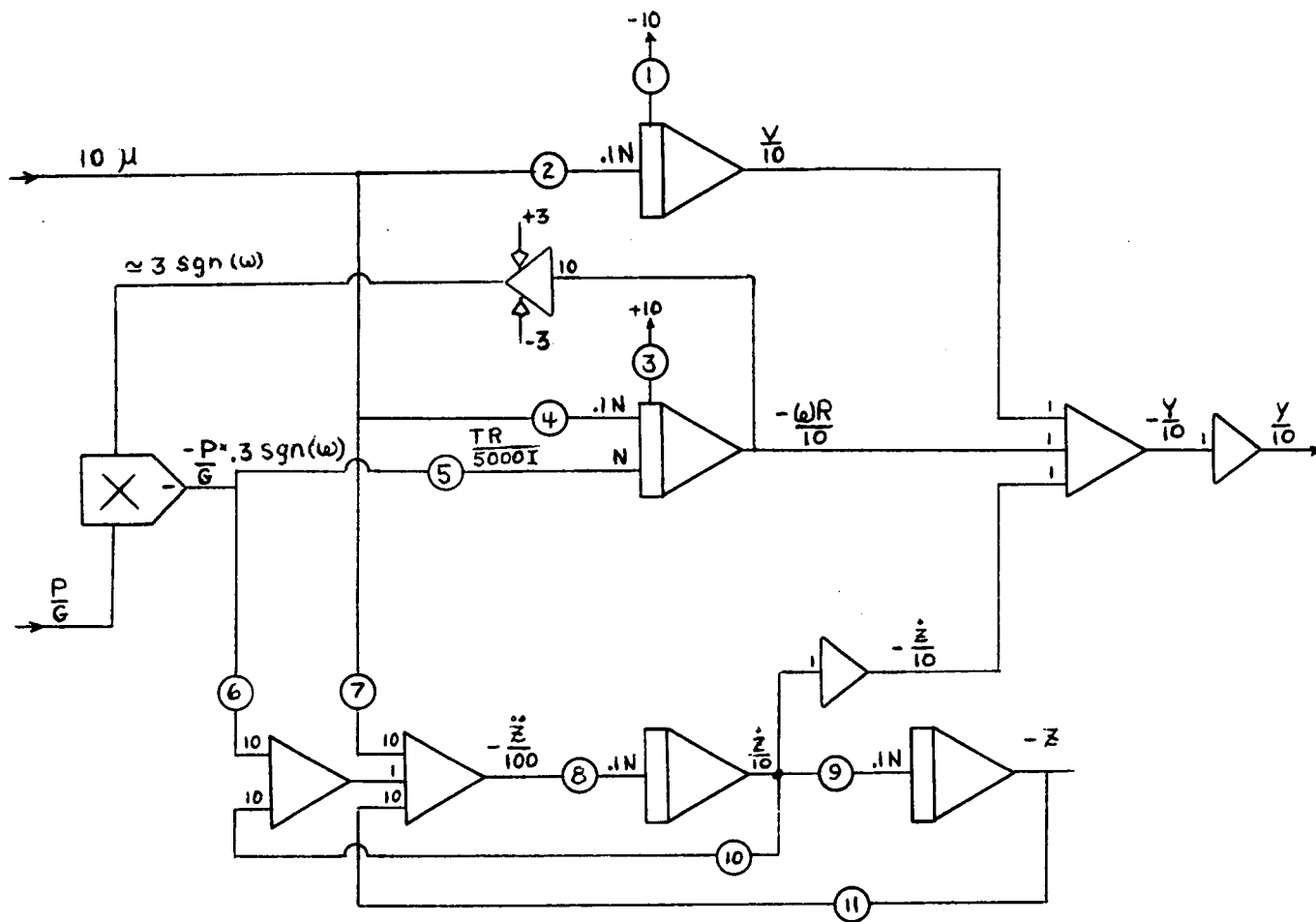


Figure A1. Scaled analog computer diagram for braking airplane.  
Vehicle dynamics.



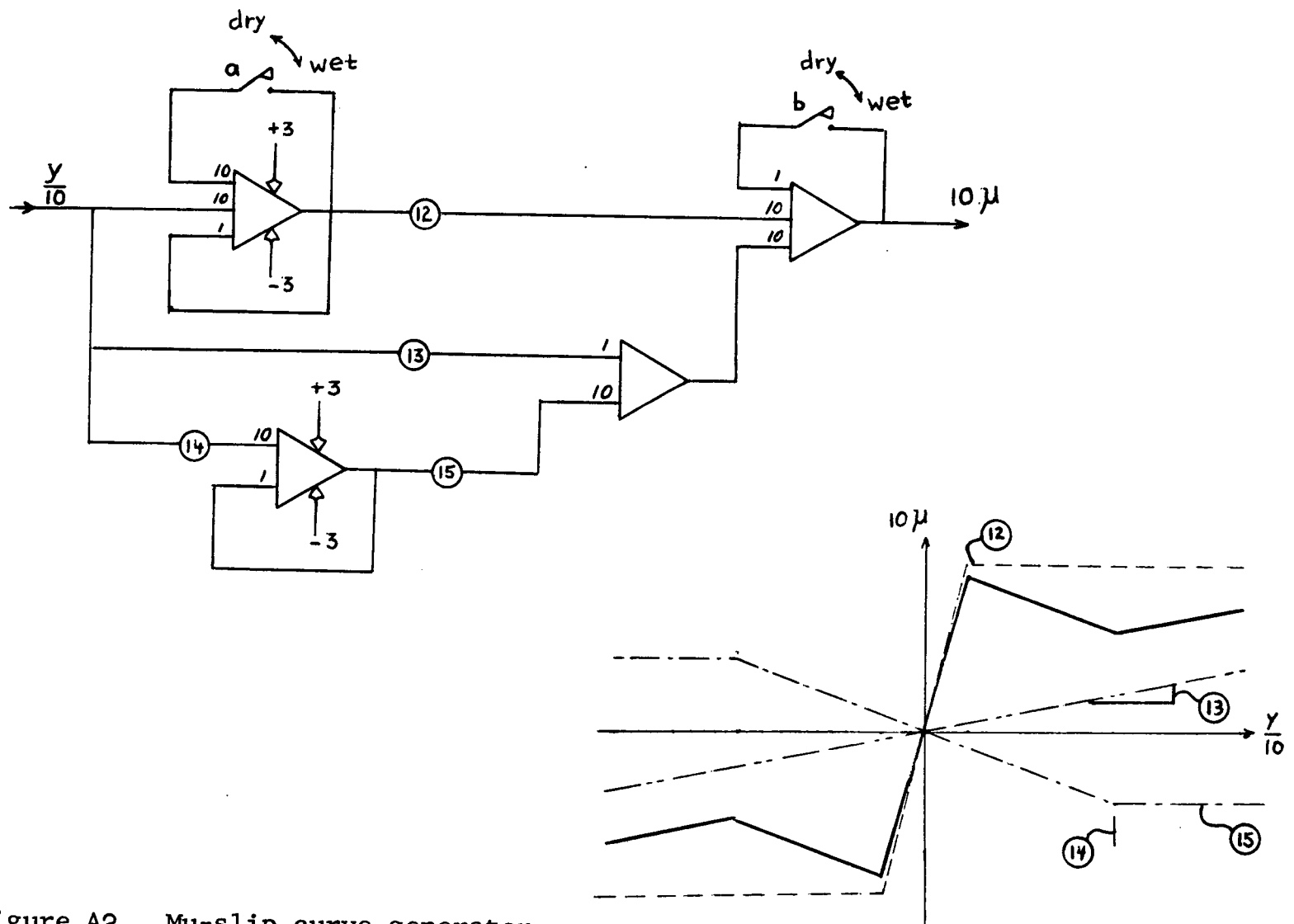


Figure A2. Mu-slip curve generator.  
 Straight line approximations show areas of curve affected by each pot. Switch a moves  $y_p$  to the right. Switch b halves effective mu.

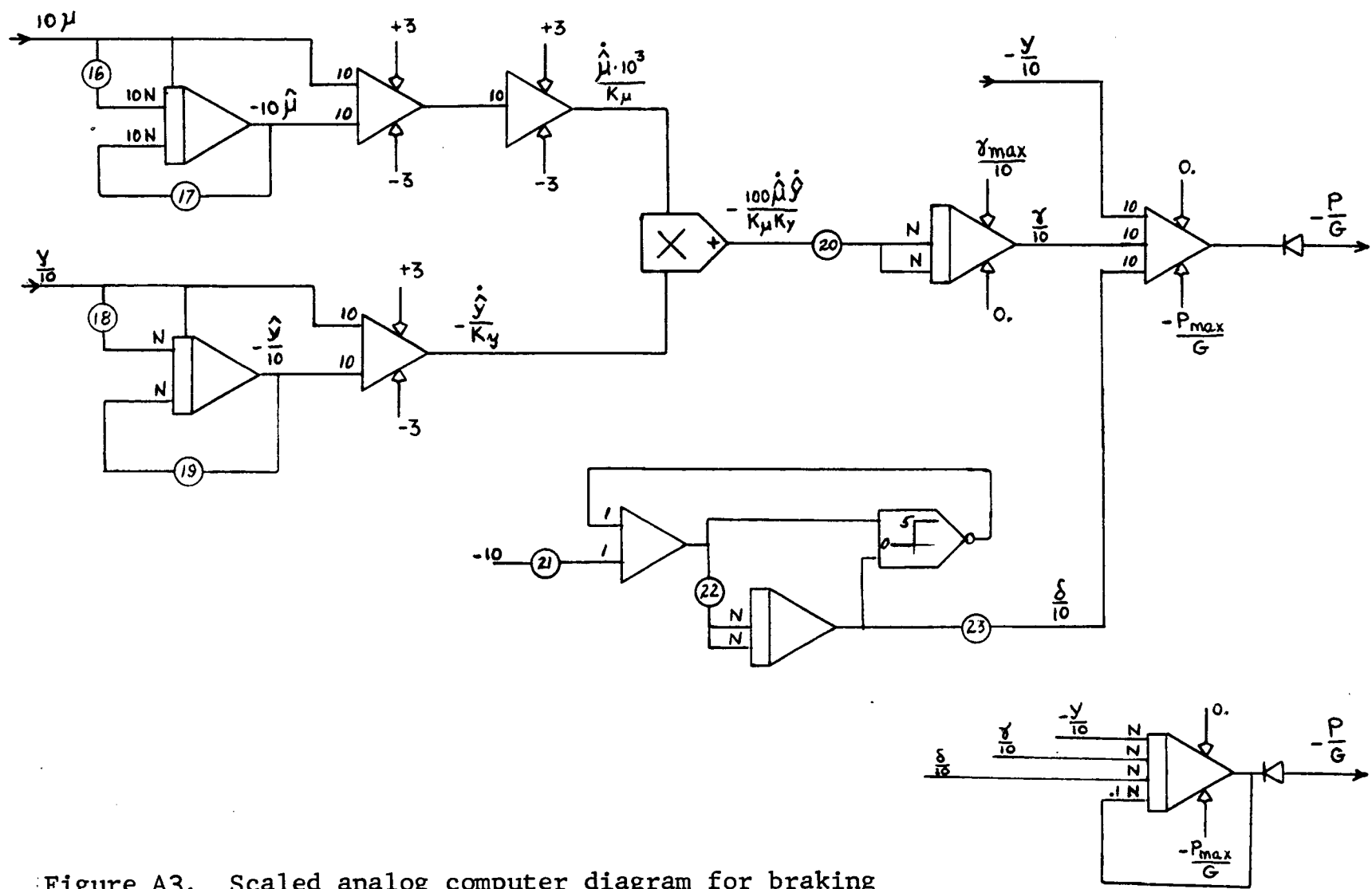


Figure A3. Scaled analog computer diagram for braking airplane. Peak-riding adaptive controller.

8 Hz. Actuator

POT NO.	SETTING	TABLE 1 DATA	CATEGORY	
1	$v(0)/100$	1.000	Process Parameters	
2	$g/5000$	.006		
3	$R \omega (0)/100$	0.		
4	$MgR^2/5000I$	1.000		
5	$GK_b R/1500I$	1.000		
6	$GK_b K_t/300M_s$	.150		
7	$Mg/M_s 10^4$	.100		
8	-	.200		
9	-	.200		
10	$C_s/100M_s$	.098		
11	$K_s/1000M_s$	.600		
12	peak-mu adj.	.330	Mu - slip Curve	
13	final slope adj.	0.		
14	min-mu slip adj.	.096		
15	kinetic mu adj.	.040		
16	$K_\mu/5000$	1.000	Controller Parameters	
17				
18	$K_y/500$	1.000		
19				
20	$K_\mu K_y K/10^6$	1.000		
21	-	.250		
22	$f_p/250 = 4/t_p (ms)$	.320		
23	$a_p/25$	.100		
REAL TIME SLOWED BY 50		N = 500 N = 10	Time-scale data	

TABLE 3. Pot settings and integrator gains.

## APPENDIX B. ADDITIONAL SIMULATION DATA

Numerous simulation runs were made to study the effect of various parameters. Because of the large distribution list for this report, actual data is not presented here to conserve reproduction costs. However, observations from this data are reported in this appendix.

### Perturbation Signal

Amplitude of the perturbation signal is not critical. As expected, the larger the perturbation, the larger the variation of slip about  $y_p$ . However, the variation of slip is not proportional to perturbation amplitude. The curvature of the mu-slip curve at the peak is the predominant factor in limiting slip variations. For example, doubling the perturbation amplitude may cause only a 10 % increase in slip variation about  $y_p$ .

On the other hand, if the perturbation amplitude is too small, the controller may drift slowly off the peak, then suddenly return to the peak after reaching a point where the slope of the mu-slip curve is large enough to correct  $\gamma$ .

Perturbation frequency is not critical, but is limited on the high side by the speed of the actuator. If the frequency is within the bandpass of the strut, then coupling with the strut dynamics causes unnecessary vibration and

fatigue, even though peak riding is still maintained. Another disadvantage of low frequency perturbation is that adaption to sudden changes in pavement conditions is necessarily slower, since the rate of change of  $\gamma$  depends heavily on the amplitude of  $\dot{y}$ .

The shape of the perturbation signal is not critical. In fact, random perturbations are quite effective, especially if high frequency noise is used. Natural noise in the actuator, tire dynamics, and/or brake lining-drum irregularities may actually be sufficient perturbation in a practical system.

#### Strut Dynamics

The strut in the simulation has a resonant frequency of about 4 hz. and a damping coefficient of about 0.2. The strut deflection in the steady state is proportional to the developed ground force. Thus, large oscillatory swings in the strut occur when sudden changes in the pavement are encountered. The adaptive controller is quite capable of peak-riding even though the strut is oscillating to and fro at rates as high as 20 ft./sec.

If, however, a pavement transient occurs at low vehicle velocity (i.e. less than 20 ft./sec.), the strut dynamics do have an effect on the peak-riding performance.

For example, if  $\dot{z} \approx v$ , then  $y$  is limited by  $v - \dot{z}$  which may be less than  $y_p$ . Fortunately, this situation is self-correcting since the developed ground force is automatically reduced for low slip, which in turn releases the strut and causes  $\dot{z} < 0$ .

#### Controller Parameters

Controller performance is affected primarily by the gain  $K$  which determines the rate at which  $\gamma$  changes. If  $K$  is too small, adaption is slow because much time is required for  $\gamma$  to reach the peak of the mu-slip curve. On the other hand, if  $K$  is too large,  $\gamma$  never reaches steady state near  $y_p$ , but oscillates about  $y_p$ .  $\gamma$  no longer functions as a set point, even though  $\gamma_{avg}$  does approach  $y_p$ . Large oscillations in  $\gamma$  essentially make the actuator operate in an on/off mode which reduces peak-riding efficiency since larger swings in  $y$  occur about  $y_p$ .

# APPENDIX C. MU - SLIP ANOMALY

Intuitively, one would expect that the coefficient of friction between tire and pavement would be dependent on slip - velocity as shown in Figure C1, where  $\mu_s$  and  $\mu_k$  are the familiar static and kinetic coefficients of friction. Figure C1 is contrary to measured mu-slip data for a rolling tire which usually produces a peak mu at other than zero slip. In an attempt to explain this anomaly, let us assume the tire-pavement characteristics in Figure C1 and generate measured mu - % slip data under the assumption of constant normal force and constant radii, when in our measurement environment such assumptions are not valid.

Consider that measurements are made from the vehicle shown in Figure C2. The rear wheels are braking wheels, while the nose wheels are non-braking or free wheels. The nose wheels will be used as the reference velocity for measuring % slip.

With  $f = dW = 0$ ,  $W_b$  and  $W_n$  assume the total weight,  $W_t$ , of the airplane (i.e.  $W_b + W_n = W_t$ ) in the ratio  $W_b/W_n = x_n/x_b$  so that the resulting torque is zero. With this weight distribution,  $W_b = c W_t$  and  $W_n = (1-c) W_t$  where  $c = x_n/(x_n + x_b)$ . The tires assume rolling radii  $R_b$  and  $R_n$  when  $W_b$  and  $W_n$  are the respective normal forces. When slip is measured experimentally from wheel tachometer readings, the rolling radii will be assumed  $R_b$  and  $R_n$  when

actually they are not. The actual rolling radii,  $r_b$  and  $r_n$ , can be more accurately expressed as

$$\begin{aligned} r_b &= R_b (1 + K_b dW/Wt) \quad \text{and} \\ r_n &= R_n (1 - K_n dW/Wt), \end{aligned} \quad (C1)$$

where  $K_b$  and  $K_n$  are dimensionless tire spring coefficients and  $dW$  is the change in weight distribution between the tires due to the developed force  $f$ .  $dW$  is the increase in nose wheel normal force and the decrease in rear wheel normal force (the total normal force remains  $Wt$ ). No dynamic response due to a sudden applied force  $f$  is considered here, only the steady state radii.

Even with  $f$  applied the moments must sum to zero:

$$\begin{aligned} f x_h - dW x_n - dW x_b &= 0, \text{ or:} \\ dW &= a f \quad \text{where } a = x_h / (x_n + x_b). \end{aligned} \quad (C2)$$

Now if  $\mu_a$  is the actual coefficient of friction, then

$$f = \mu_a (W_b - dW). \quad (C3)$$

Under the assumption that the rear wheel normal force is  $W_b$  (it is actually  $W_b - dW$ ),  $\mu$  would be measured as:

$$\mu_m = f/W_b. \quad (C4)$$

(C2) and (C3) can be solved simultaneously for  $dW/W_b = a\mu_a/(1+a\mu_a)$  and  $f/W_b = \mu_a/(1+\mu_a)$ . Thus, the measured  $\mu$  is related to actual  $\mu$  by:

$$\boxed{\mu_m = \frac{\mu_a}{1 + a \mu_a}} \quad \text{where} \quad \boxed{a = \frac{x_h}{x_n + x_b}}. \quad (C5)$$

At this point we also have:

$$dW/Wt = ac\mu_a/(1+ac\mu_a) \quad \text{where} \quad \boxed{c = \frac{x_n}{x_n + x_b}}. \quad (C6)$$

Now, the actual tire slip ratio is  $v/V$  where  $v$  is the



relative velocity between tire and pavement and  $V$  is the airplane velocity. Since the nose wheels are not slipping,  $V = \omega_n r_n$ . Also,  $v = \omega_n r_n - \omega_b r_b$ . Thus:

$$\frac{v}{V} = 1 - \frac{\omega_b r_b}{\omega_n r_n} \quad \text{or} \quad \frac{\omega_b r_b}{\omega_n r_n} = 1 - \frac{v}{V} . \quad (C7)$$

On the other hand, assuming constant radii and measuring the angular wheel speeds, measured slip ratio is

$$\sigma_m = 1 - \frac{\omega_b R_b}{\omega_n R_n} . \quad (C8)$$

(C7) into (C8) gives an alternate expression:

$$\sigma_m = 1 - \left(1 - \frac{v}{V}\right) \frac{R_b}{r_b} \frac{r_n}{R_n} . \quad (C9)$$

(C1) into (C9) gives still another:

$$\sigma_m = 1 - \left(1 - \frac{v}{V}\right) \frac{1 - K_n dW/Wt}{1 + K_b dW/Wt} ; \quad (C10)$$

and finally, (C6) into (C10) gives  $\sigma_m$  as a function of actual mu-slip data:

$$\sigma_m = 1 - \left(1 - \frac{v}{V}\right) \frac{1 + a\mu_a(1 - cK_n)}{1 + a\mu_a(1 + cK_b)} . \quad (C11)$$

Thus (C5) and (C11) where  $c$  is defined in (C6) give the transformation from actual mu-slip data to measured (under faulty assumptions) mu-slip data.

As an example, let the airplane data be:  $a=0.4$ ,  $c=0.9$ ,  $K_b=.05^*$  and  $K_n=.5^*$ . Let us now transform the curve of Figure C1 with  $\mu_s=1.0$ ,  $\mu_k=0.5$ , and  $v_k=10$  ft/sec into measured mu-slip data for airplane speeds of  $V=100, 50$ , and

F

20 ft/sec.

The above data into (C5) and (C11) produces the curves shown in Figure C3. Note that the entire portion of the curve from  $\sigma_m=0$  to peak  $u_m$  was generated by  $v=0$  and is independent of  $V$ , the velocity of the airplane. Hence, the measured slip at which the peak  $\mu$  occurs is dependent only upon airplane geometry (i.e.  $a$  and  $c$ ); tire elasticity, inflation, temperature, etc. (i.e.  $K_n$  and  $K_b$ ); and the static coefficient of friction between tire and pavement (i.e.  $\mu_s$ ) which is also a function of tire inflation, temperature, etc. along with pavement conditions (i.e. wet, dry, ice, etc.). The remainder of the measured  $\mu$ -slip curve is dependent upon airplane velocity along with all of the aforementioned factors.

The above argument supports the hypothesis that typical  $\mu$ -slip curves used by investigators in braking studies may be more dependent upon measurement methods (and assumptions) than upon the actual physical phenomena. However, experimentation is necessary before concluding that the above argument offers even a partial explanation of the  $\mu$ -slip anomaly.

---

\* Note that  $K_b=.05$  implies that the rear tire rolling radius would increase 4.5% if the entire load  $W_b=.9W_t$  were removed. Also,  $K_n=.5$  implies that the front tire rolling radius would decrease 5% if its steady load of  $W_n=.1W_t$  were doubled.

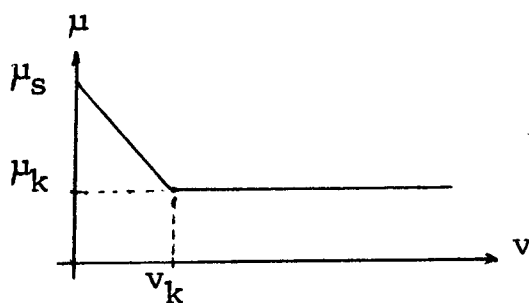


Figure C1. Coefficient of friction vs. relative velocity between two surfaces.

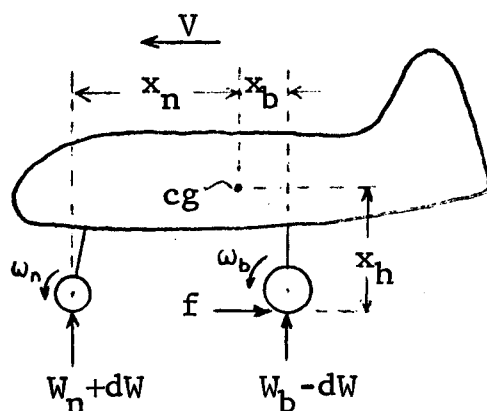


Figure C2. Braking airplane.

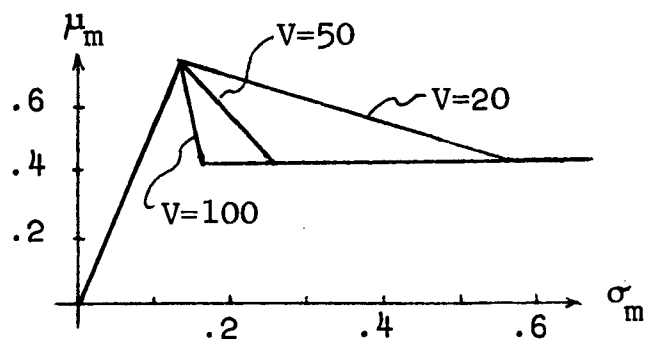


Figure C3. Measured mu-slip (ratio) data.